

Corrosion Behavior of WC-FeCrAl Coatings Deposited by HVOF and HVAF Thermal Spraying Methods

I. Hulka^{*}, D. Utu^{*}, V.A. Serban^{*}, M.L. Dan^{*}, V. Matikainen^{**} and P. Vuoristo^{**}

^{*} Politehnica University of Timisoara, P-ta Victoriei, Nr 2, 300006, Timisoara, Romania, email: iosif.hulka@upt.ro

^{**} Tampere University of Technology, Department of Materials Science, FI-33720, Finland

Abstract: The present work compares the mechanical properties and corrosion resistance of WC-FeCrAl coatings manufactured using high-velocity oxygen fuel (HVOF) technology equipped with DJ2700 spraying gun and high-velocity air fuel (HVAF) equipment using M3 supersonic spraying gun. The results indicated that decarburization of carbide phase occurred in both. It was found out that the deposition velocity is an important factor influencing the density of the coating and thus the amount of porosity. The HVAF sprayed WC-FeCrAl coating revealed the lowest degree of porosity, higher hardness and lower degree of decarburization, achieving the best properties in terms of electrochemical corrosion resistance compared to HVOF sprayed coating.

Keywords: Hard coatings, cermet, carbides, WC-FeCrAl, HVOF and HVAF spraying, corrosion studies.

1. Introduction

Thermally sprayed coatings have been increasingly applied in various industrial fields to provide protection against wear and corrosion. The spraying process involves the deposition of molten or semi-molten powder particles onto a certain substrate to form a protective coating. High velocity oxy-fuel spraying (HVOF) is a relatively new thermal spraying method used to deposit different types of protective coatings [1]. In the spraying process the fuel is burnt with oxygen at high pressure generating a high velocity jet. During spraying the gas velocity is over 750 m/s and gas temperature 2200-3200 [2]. The temperature is lower compared to some other thermal spraying processes like plasma spraying, which is beneficial when cermet coatings are deposited due to decreased decarburization by the lower temperature. The particle velocity and process temperature depend on the gas mixture used in the deposition process.

Compared to HVOF spraying, high velocity air-fuel (HVAF) spraying is a recently developed technology for the deposition of powders which are heated below their melting point during spraying and accelerated to velocities from 700 m/s up to 1200 m/s and temperatures under 2000 °C [3]. The newly obtained coatings are dense with minimal thermal degradation. The process is a solid particle technology where particle temperature during spraying is an important factor in coating manufacturing [4]. Both HVOF and HVAF processes are used to manufacture composite, hard-face metal, metallic alloys, cermet and other coatings in order to extend the lifetime of components which operate in harsh environments [5, 6].

This work aims to investigate the influence of the deposition process on the microstructure of the HVOF and HVAF sprayed WC-FeCrAl coatings in terms of mechanical characteristics and corrosion behavior.

2. Experimental

The coatings were deposited onto low carbon steel substrates using a M3 HVAF (Uniqucoat Technologies LLC, US) spray gun and a DJ2700 HVOF gun (Sulzer Metco, US). Commercially available WC-FeCrAl powder was used as a feedstock material (H.C. Starck, Germany). The powder has a nominal particle size distribution in the range of 15-45 µm and the following chemical composition: C ~ 5.6%, Fe ~ 11%, Cr ~ 3.3%, Al ~0.9% and W in balance. The low carbon substrates were grit-blasted with alumina before spraying in order to increase the surface roughness. The average particle in-flight velocities and temperatures were measured with Spraywatch 4s camera (Oseir Ltd., Finland) from the spray distance (300 mm). The cross-sections of the sprayed coatings were examined with a Quanta FEG 250 (FEI, The Netherlands) scanning electron microscope (SEM) equipped with EDAX analyzer.

X-ray diffractometry (XRD) of powder and as-sprayed coatings was performed on a Empyrean diffractometer (PANAnalytical, The Netherlands) using Cu-Kα radiation. The measurements were performed at 2θ diffraction angle in the range of 20°–100° and step size 0.02°. Phase identification was performed using the PANAnalytical X'Pert High Score Plus software using the ICDD JCPDF-2 database (International Centre for Diffraction Data, Newtown Square, US). The porosity of the coatings was determined by image analysis using image processing software, Image Tool 3.00, onto 10 backscattered electron micrographs at 1000X magnification. The roughness of the as-sprayed coatings was investigated with a Mitutoyo SJ 201 roughness tester and micro-hardness measurements were performed with a Matsuzawa MMT X7 tester using 300g load.

The electrochemical tests included potentiodynamic

polarization studies (Tafel polarization method) and Electrochemical Impedance Spectroscopy (EIS) measurements. The tests were performed at 25°C temperature on a SP-150 potentiostat/galvanostat (Bio-Logic, SAS, France) using a typical glass cell equipped with three electrodes: Ag/AgCl as reference electrode, working electrodes consisting of WC-FeCrAl HVOF and HVOF sprayed samples and a platinum mesh used as counter electrode. The open circuit potential was measured after 60 minutes of immersion of the coatings in the NaCl 3.5% solution for potential stabilization. For the experiments the exposed surface of samples was 1 cm².

3. Results and Discussion

3.1. Powder characterization

The WC-FeCrAl powder (H. C. Starck, Germany) used in the present study is a commercial powder having the morphology and chemical composition presented in Figure 1. The blocky WC carbide particles are embedded in a Fe-Cr-Al metallic binder and form powder particles with rounded morphology characterized by pores, entrances and voids. From the particle cross-section image (Fig. 1c) and according to the EDX quantification, the metallic matrix, which is a mixture between Fe-Cr-Al, is characterized by

light gray areas (label 1), Cr rich areas represented by dark gray shades (label 2) while the carbide zones show up very bright (label 3).

3.2. Coating microstructure

Polished cross-sections of the coatings were analyzed by SEM and are presented in Figure 2. Both coatings exhibit dense microstructure free of major defects and reduced porosity. WC particles showed up very bright in the SEM images, while the metallic matrix has different shades of gray, depending on the amount of Fe, Cr and Al. The HVOF sprayed WC-FeCrAl coating presents a higher degree of dissolution and oxidation and as a result the carbides within the coating look more rounded compared to the coating deposited by HVOF method where the carbides are still blocky due to reduced dissolution and oxidation caused by the spraying process [7]. From SEM images it can be noticed that the coatings present similar morphologies but still some differences can be noticed. Thus, the degradation of the carbide phase is more severe in the HVOF sprayed coating compared to the HVOF sprayed one. A larger amount of fine carbides are retained in the HVOF coating and they exhibit angular morphologies.

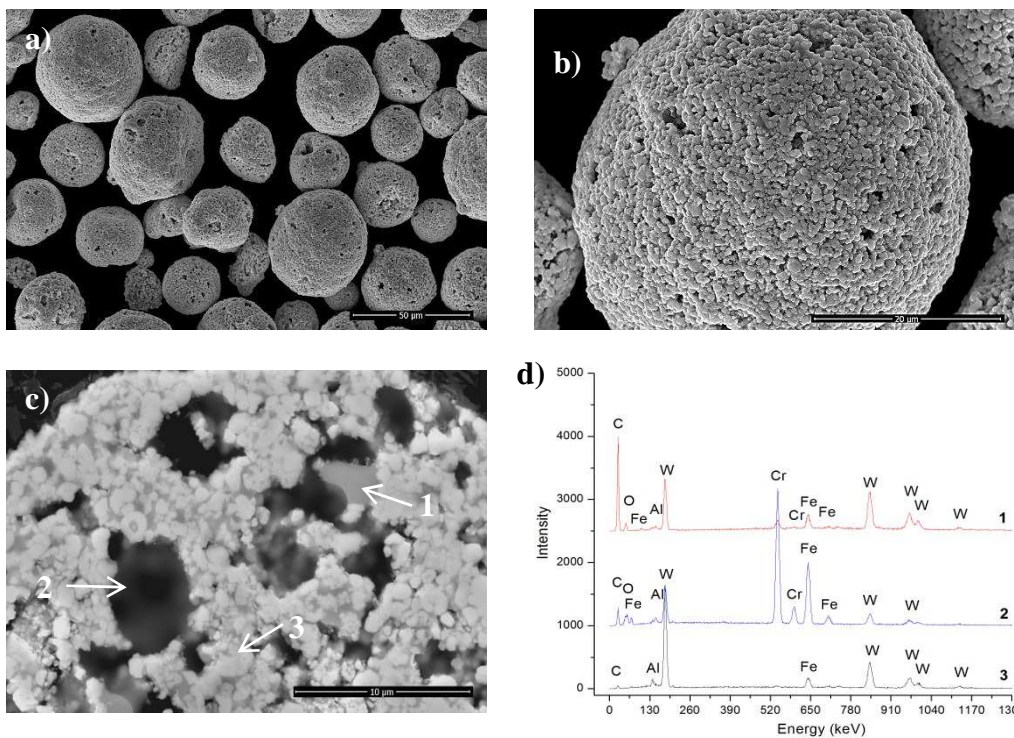


Figure 1. Micrographs of morphology of WC-FeCrAl powder (a), single powder particle (b); powder particle cross-section (c) and EDX spectra of powder (d)

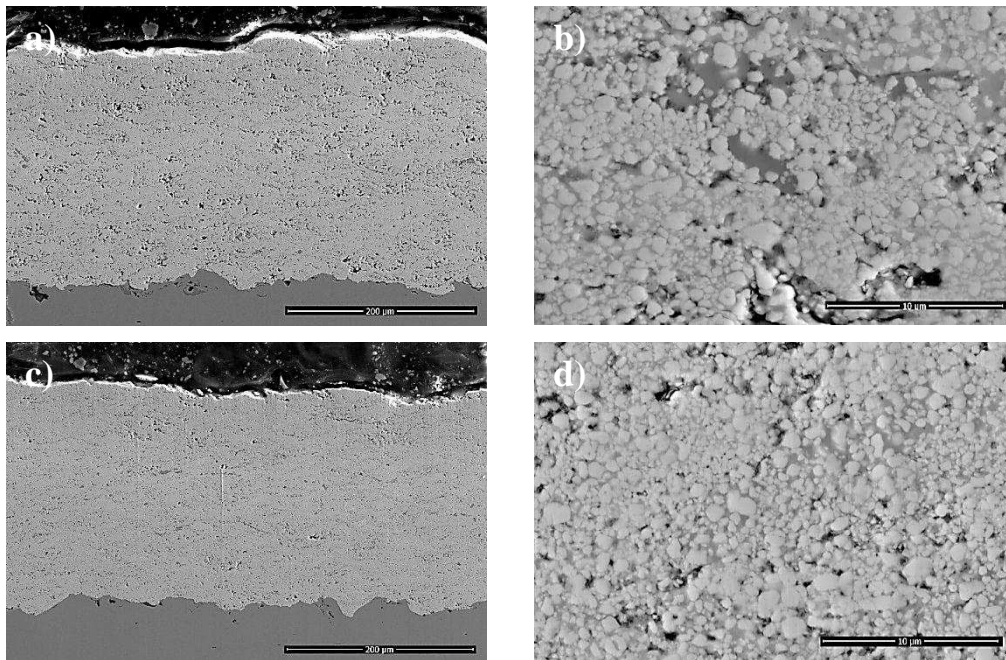


Figure 2. SEM micrographs of HVOF (a, b) and HVAF (c, d) sprayed WC-FeCrAl

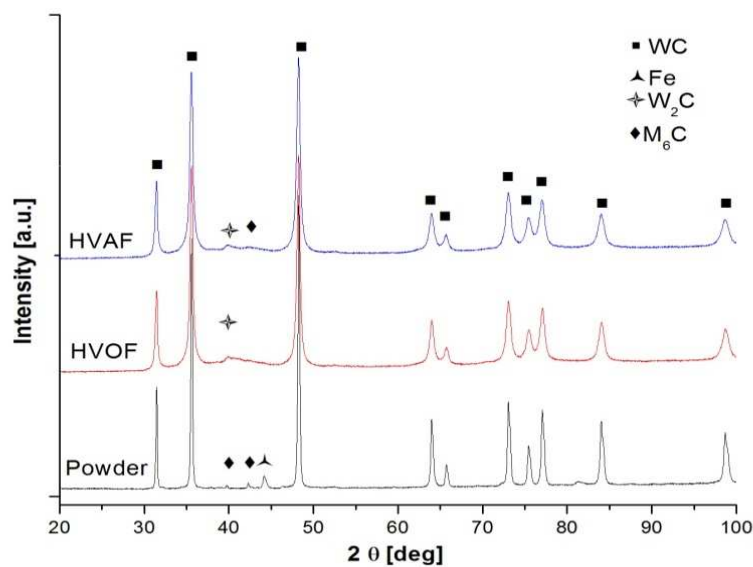


Figure 3. X-ray diffraction patterns of the investigated WC-FeCrAl powder and sprayed coatings

The XRD patterns of feedstock powder and thermally sprayed coatings are presented and compared in Figure 3. The pattern of the powder indicated the presence of WC as major peaks along with the signals ascribed to Fe and M_6C which represents Fe, Cr and Al rich areas. Both coatings exhibit primary phases of WC together with small amounts of W_2C . In both coatings the lack of Fe peak might be noticed. The dissolution of carbides into the metallic matrix (Fe-Cr-Al) can cause the formation of carbon saturated metal matrix, amorphous phases and nano-crystalline phases. The slight "hump" which can be seen around 40-45 degrees might be assumed to be caused by amorphous phases. The absence of M_6C phase in the HVOF coating

might be noticed as well due to a more extensive melting of the matrix phase occurred due to higher process temperature during spraying.

Table 1 presents the results of the measured coating thickness, micro-hardness, surface roughness and porosity. The thickness and roughness of both thermally sprayed coatings have similar values but differences can be noticed in the micro-hardness and porosity values. The HVAF sprayed coating showed higher hardness and reduced porosity compared to the HVOF sprayed coating which might be attributed to the higher average velocity of the sprayed particles leading to denser coatings.

TABLE 1. Thickness, hardness, roughness and porosity of thermally sprayed WC-FeCrAl coatings

	Coating thickness [μm]	Micro-hardness HV0.3	Roughness Ra [μm]	Porosity [%]	Particle velocity [m/s]	Particle temperature [C]
HVOF	229 \pm 14	878 \pm 191	5.414 \pm 0.31	1.64	621	1780
HVAF	235 \pm 5	1169 \pm 89	4.344 \pm 0.40	0.84	852	1510

3.3. Corrosion behavior

3.3.1 Potentiodynamic polarization studies

The evolution in time of the equilibrium potential of WC-FeCrAl coatings was studied and after 1 testing hour, when the system had reached a quasi-stationary state, linear polarization measurements were recorded. Potentiodynamic polarization enables fast corrosion rate determination via the intensity of the corrosion current and Tafel slopes. It also shows possible changes which might occur at the electrode surface or changes in the mechanism of corrosion process.

In the present paper, a sweep potential of ± 250 mV was applied against the open circuit potential and a scan speed of 1 mVs^{-1} was used. By this method the corrosion rate can be calculated using the direct substitution of Tafel slope values (cathodic - b_c and anodic - b_a) using the following equation:

$$i = i_{cor} \left\{ \exp \left[\frac{2,303}{b_a} (E - E_{cor}) \right] - \exp \left[- \frac{2,303}{b_c} (E - E_{cor}) \right] \right\} \quad (1)$$

where $\frac{2,303}{b_a}$ represent the anodic slope and $\frac{2,303}{b_c}$ respectively the cathodic slope; Tafel slope constants associated with anodic (b_a) and cathodic (b_c) processes; E and E_{cor} - potential and corrosion potential; i_{cor} - corrosion current density. Linear polarization curves recorded for WC-FeCrAl coatings deposited by HVOF and HVAF thermal spraying in 3.5% NaCl at 25°C are presented in Figure 4.

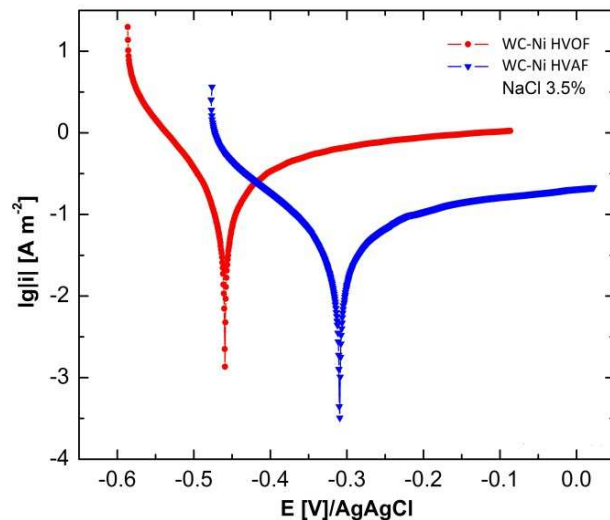


Figure 4. Polarization curves of the WC-FeCrAl coatings

In order to determine the electrochemical parameters the polarization curves were fitted and the results are presented in Table 2. The HVAF coating exhibits better corrosion resistance indicated by the lower passive current density and wide passive region due to a denser coating as a result of reduced porosity and micro-cracking. Also, the higher hardness compared to the HVOF coating might have a positive effect on the corrosion behavior of HVAF sprayed WC-FeCrAl coating.

SEM studies of the corroded surfaces of thermally sprayed coatings presented in Figure 5 reveal that noticeable pitting corrosion occurred during the tests at the metallic matrix border. The electrolyte attacked firstly the softer phases which conducted in time to carbide fall-outs.

TABLE 2. Electrochemical parameters obtained from the polarization curves

TS Process	$M_{echiv.}$ [g]	$Dens.$ [g cm ⁻³]	i_{cor} [$\mu\text{A cm}^{-2}$]	E_{cor} [mV]	$-b_c$ [mV dec ⁻¹]	b_a [mV dec ⁻¹]	R_p [Ω]	v_{cor} [mm an ⁻¹]
HVOF	40.56	4.3	13.33	-461	84	173	1283	0.41
HVAF	40.56	4.3	3.43	-309	126	234	8167	0.09

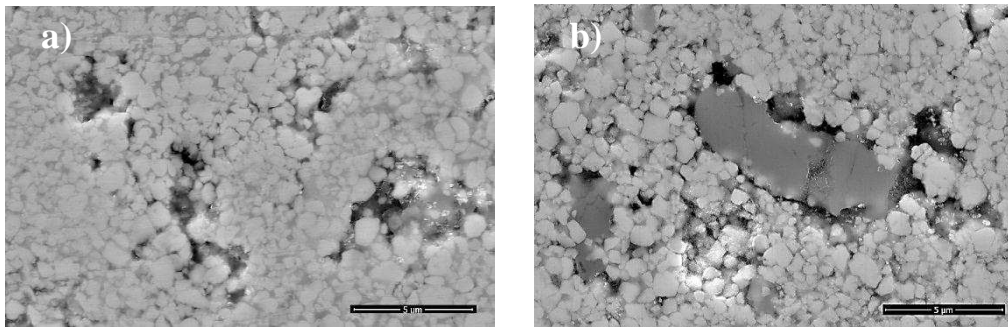


Figure 5. SEM micrographs of HVOF (a) and HVAF (b) coatings after corrosion test in 3.5% NaCl solution at 25°C

3.3.2 Electrochemical Impedance Spectroscopy

The results of EIS measurements are expressed by so called Nyquist and Bode diagrams [8, 9] presented in Figure 6. The Nyquist plot for the HVAF coating shows the presence of an incomplete semicircle attributed to a depressed capacitive loop at high to intermediate frequency range [9]. Capacitive loop appear from the time constant of the electrical double layer and can be associated with charge transfer resistance [10]. In the case of corrosion, the polarization resistance of the working electrode depends on the micro-cracks and porosity within the coating. Deviation of the recorded circle from the perfect circular shape can be associated with electrode superficial inhomogeneity, which might be noticed for the HVOF coating. This superficial inhomogeneity appears as the effect of surface roughness or different interfacial phenomena. Equivalent circuit for

spectra fitting (Figure 7) was recorded based on the Nyquist and the Bode diagrams.

When analyzing the equivalent circuit presented in Figure 7 it can be observed that the system consists of four components: R_s – solution resistance, CPE – constant phase element which represents a modified capacitance that is a frequency dependent element and is related to the surface roughness [11], R_{ct} – charge transfer resistance and W – Warburg impedance which is associated with mass transport process. Warburg impedance suggested that the corrosion reaction during the test is limited by mass transport. Electrical circuit used for modeling of experimental EIS data consist of a serial connection between solution resistance (R_s) and a parallel connection of the constant phase connection (CPE) and the charge transfer resistance (R_{ct}) in series with a Warburg impedance.

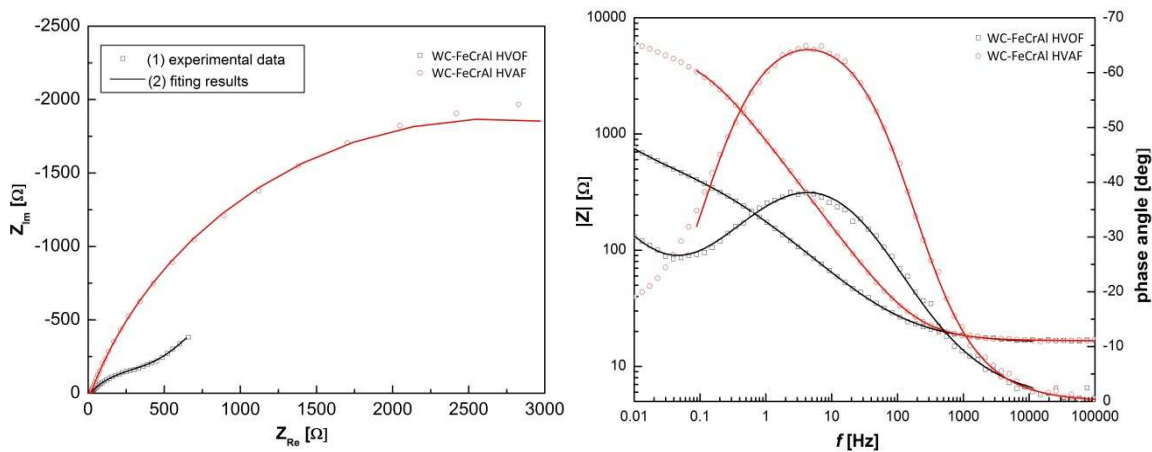


Figure 6. Nyquist (a) and Bode (b) plots obtained in NaCl 3,5% solution at 25°C for WC-FeCrAl thermally sprayed coatings

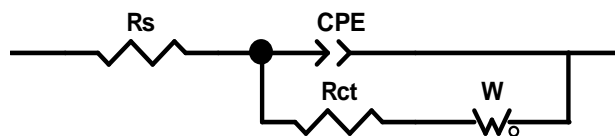


Figure 7. Equivalent circuit for spectra fitting

TABLE 3. Experimental values of EIS during the corrosion process

TS process	R_s [$\Omega \text{ cm}^2$]	T [$\text{F cm}^{-2} \text{ s}^{n-1}$]	n	R_{ct} [$\Omega \text{ cm}^2$]	C_{dl} [$\mu\text{F cm}^{-2}$]	Chi^2
HVOF	15,98 (0,48%)	$14,9 \cdot 10^{-4}$ (2,85%)	0,59 (0,82%)	337,1 (0,88%)	101	$4,5 \cdot 10^{-4}$
HVAF	16,6 (0,41%)	$2,55 \cdot 10^{-4}$ (0,73%)	0,78 (0,21%)	5327 (1,57%)	544	$1,6 \cdot 10^{-4}$

The impedance of the constant phase element is described by:

$$Z_{CPE} = \frac{1}{T} (j\omega)^n \quad (2)$$

where $0 < n < 1$ - represents the constant phase angle of CPE, T is a parameter related to the double layer capacitance [12]. Impedance of Warburg element in case of a finite length thickness of diffusion layer δ can be expressed:

$$Z_w = (R_w(j\omega\tau_D)^{-\phi}) \tan(j\omega\tau_D)^\phi \quad (3)$$

where R_w - diffusion resistance; τ_D - diffusion time constant given by $\tau_D = \delta^2/D$, where δ - diffusion thickness and D - diffusion coefficient; ϕ - an exponent with values between 0 and 1 [12].

After modeling of experimental data for both superficial layers the results are presented in Table 3. The charge transfer resistance is associated with the occurrence of the charge transfer reaction at due to the pores and micro-cracks found within the coating. The HVAF coating has higher R_{ct} value compared to the HVOF coating, which can be attributed to the more effective barrier behavior.

EIS measurements therefore show that the HVAF coating possess less interconnected porosity and micro-cracks which indicates through electrochemical characteristics that the coating is nobler than HVOF coating.

4. Conclusions

From the present study the following conclusions can be drawn:

- Dense, homogenous and hard coatings were obtained from the WC-FeCrAl feedstock material with both HVOF and HVAF spraying processes;

- The HVAF process produced higher average particle velocity compared to HVOF spraying. This resulted in denser and harder coating structure;

- Both coatings exhibit primary phases of WC together with small amounts of W_2C . The HVOF coating exhibits the largest decarburization and presents a broader W_2C peak which indicates higher dissolution of carbide phase during spraying while the HVAF coating is less

decarburized. This can be attributed to lower process and particle temperature in the HVAF spray process;

- The diffraction peaks of the metallic iron-based phase were not detected in the as-sprayed coatings. This is most likely caused by the rapid cooling during spray process resulting in amorphous or nanocrystalline structure;

- The corrosion tests indicated that the HVAF sprayed WC-FeCrAl coating is nobler and presents a better corrosion behavior in 3.5% NaCl solution at 25°C.

ACKNOWLEDGEMENT

This work was supported by the strategic grant POSDRU/159/1.5/S/137070 (2014) of the Ministry of National Education, Romania, co-financed by the European Social Fund - Investing in people, with the Sectorial Operational Program Human Resources Development 2007-2013.

REFERENCES

- Verstak A., Baranovski V., Thermal Spray 2003: Advancing the Science and Applying the Technology, ASM International, **2003**, 535-541.
- Davis J.R., Handbook of Thermal Spray Technology, ASM International, **2004**.
- Uniquecoat Technologies Inc., website: www.uniquecoat.com
- Tao K., Zhang J., Cui H., Zhou X.L. and Zhang J.S., *Transactions of Nonferrous Metals Society of China*, **18**, **2008**, 262-269.
- Kermetico, website: www.kermetico.com
- Voronetski A., Belashchenko V., Thermal Spray 2006: Science, Innovation, and Application (ASM International), **2006**, 637-642.
- Bolelli G., Borner T., Milanti A., Lusvarghi L., Laurila J., Koivuluoto H., Niemi K. and Vuoristo P., *Surface and Coatings Technology*, **248**, **2014**, 104-112.
- Orazem M.E. and Tribollet B., Electrochemical impedance spectroscopy, Ed. Wiley, **2008**.
- Barsoukov E. and Macdonald J.R., Impedance spectroscopy theory, Experiment and Applications, Ed. Wiley Interscience, **2005**.
- Ashassi-Sorkhabi H., Ghalebsaz-Jeddi N., Hashemzadeh F. and Jahani, H., *Electrochimica Acta*, **51**, **2006**, 3848-3854.
- Lecante A., Robert F., Blandinieres P.A. and Roos C., *Current Applied Physics*, **11**, **2011**, 714-724.
- Kellenberger A. and Vaszilcsin N., Micro si Nanomateriale: Electrochimia starii solide, Ed. Politehnica, **2013**.

Received: 08 November 2015

Accepted: 02 December 2015